IEEE Photonics Journal
An IEEE Photonics Society Publication

Open Access

Investigation of Q-Switched and Mode-Locked Pulses From a Yb^{3+}-Doped Germano-Zirconia Silica Glass Based Fiber Laser

Volume 9, Number 4, August 2017

Wei-Cheng Chang
Yu-Sheng Lin
Yin-Wen Lee
Chien-Hsing Chen
Ja-Hon Lin
Pinninty Harshavardhan Reddy
Shyamal Das
Anirban Dhar
Mukul Chandra Paul

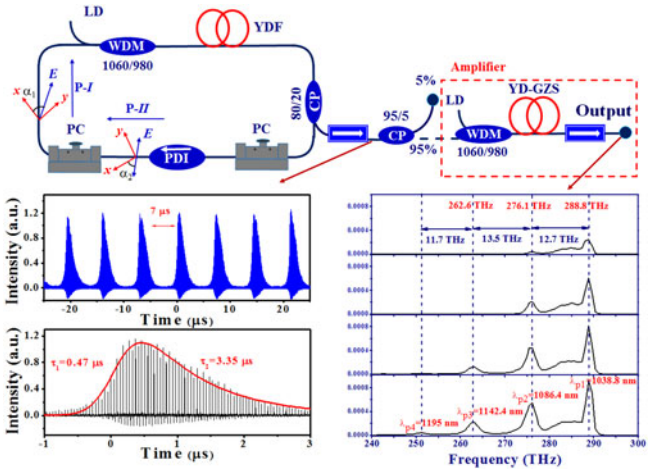

DOI: 10.1109/JPHOT.2017.2718020
1943-0655 © 2017 IEEE

Investigation of Q-Switched and Mode-Locked Pulses From a Yb^{3+}-Doped Germano-Zirconia Silica Glass Based Fiber Laser

Wei-Cheng Chang,[1] Yu-Sheng Lin,[1] Yin-Wen Lee,[1] Chien-Hsing Chen,[1] Ja-Hon Lin,[1] Pinninty Harshavardhan Reddy,[2,3] Shyamal Das,[3] Anirban Dhar,[3] and Mukul Chandra Paul[3]

[1]Department of Electro-Optical Engineering, and Institute of Electro-Optical Engineering, National Taipei University of Technology, Taipei 10608, Taiwan
[2]Academy of Scientific and Innovative Research, CSIR-CGCRI Campus, Kolkata 700032, India
[3]CSIR-Central Glass and Ceramic Research Institute, Kolkata 700032, India

DOI:10.1109/JPHOT.2017.2718020

Manuscript received April 24, 2017; revised June 16, 2017; accepted June 16, 2017. Date of publication July 26, 2017; date of current version August 8, 2017. This work was supported in part by the Ministry of Science and Technology of Taiwan, under Grants MOST 105-2112-M-027-001-MY3 and MOST 105-2221-E-027-054, and financial support for the development of the YD-GZS fiber was supported in part by the Department of Science and Technology, New Delhi, India. Corresponding author: Ja-Hon Lin (e-mai: jhlin@ntut.edu.tw).

Abstract: The Q-switched and mode-locked (QML) pulses of an all normal dispersion Yb^{3+}-doped fiber laser (YDFL) using the nonlinear polarization rotation technique with symmetric and asymmetric Q-switched envelopes were investigated. For QML pulses with a symmetric shape, the width of envelope decreases as the pump power increases, achieving a shortest duration of $\sim$1.4 μs. An alternate QML state of the YDFL exhibited an asymmetric envelope with a broad spectrum bandwidth, and whose short duration mode-locked pulses could be used as a light source for the cascaded Raman scattering generation through the injection of these high intensity QML pulses into an amplifier, using Yb^{3+}-doped germano-zirconia silica (YD-GZS) glass based fiber as the gain fiber. In addition, the generation of a relatively broad spectrum near the IR range and the observation of some emission bands in the visible and UV range have been demonstrated at high pump power.

Index Terms: Q-switched and mode-locked, Supercontinuum generation, Yb^{3+}-doped fiber laser.

1. Introduction

Recently, passively mode-locked lasers (PMLs) operating within near-infrared range (e.g., diode pump solid state lasers (DPSSLs), and fiber laser systems), have attracted considerable attention, since they can be widely used in industrial applications, medical diagnosis and scientific investigations. PMLs have been experimentally demonstrated with the insertion of a saturable absorber (SA) such as the semiconductor saturable absorber mirror (SESAM) [1], carbon nanotubes or graphene [2], and graphene oxide inside laser cavity [3]; or with artificial SAs, such as the nonlinear amplifier loop mirror (NALM) [4] and nonlinear polarization rotation (NPR) methods [5]. In general, the repetition rate of a continuous wave mode-locked (CW-ML) pulse train from conventional PMLs,

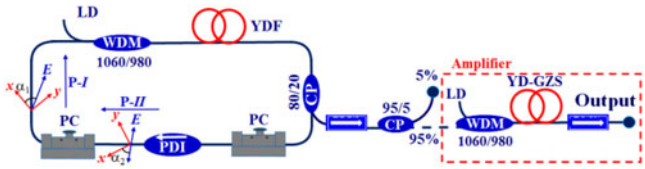

Fig. 1. Schematic setup of PML YDFL (WDM: wavelength-division-multiplexing coupler; YDF: ytterbium-doped fiber; PDI: polarization dependent isolator; PC: polarization controllers) and the YDFA using the YD-GZS as a gain fiber.

which is determined by the cavity length, is relatively high. By using these CW-ML lasers in some nonlinearity measurements, it can induce undesirable effects such as the thermal lensing effect or even cause damage to the samples. Therefore, it has become of crucial importance to reduce the pulse repetition rate and to increase the pulse energy of CW-ML pulses through technological means such as cavity dumping, pulse pickers, or even the regenerative amplifying system. The Q-switched and mode-locked (QML) technique is an alternative way to achieve this goal that has been demonstrated in DPSSLs by using Cr^{4+}:YAG as a saturable absorber [6] and ytterbium-doped fiber lasers (YDFLs) through the insertion of the SESAM inside the laser cavity, or by adopting the NPR technique [1], [7], which we have used here.

In recent decades, supercontinuum generation (SCG) produced by launching high peak-power, ultra-short optical pulses through highly nonlinear fibers, such as photonic crystal fibers [8], [9], and tapered fibers [10], [11], has also attracted great interest. The produced supercontinuum spectra typically exhibit broad bandwidths, which can be over hundreds or even thousands of nanometers, with fine inner structures and can be practically applied in a number of areas, such as optical frequency metrology, spectroscopy, optical coherence tomography, and optical communications [12]. The mechanism of SCG has been attributed to various nonlinear phenomena including self-phase modulation (SPM), stimulated Raman scattering (SRS), four-wave mixing, soliton fission, Raman self-frequency shifts, and dispersive wave generation [13]. Owing to their compact structure and reliable properties for use as an all fiber SCG source, several active media, such as Yb-doped fibers with emission wavelength of $\sim$1 μm [14], [15] and Er-doped fibers with emission wavelength of $\sim$1.55 μm [16], [17], have been adopted for use as ultra-broad light sources. The evolution of SCG by launching a low repetition rate CW-ML pulses from an all-normal-dispersion (ANDi) YDFL into a ytterbium doped amplifier (YDFA), through YD-GZS fibers, has been recently demonstrated [18]. In this work, we investigated the soliton dynamics of YDFL, focusing particularly on the characteristics of QML pulses. After launching QML pulses through the YDFA, cascaded Raman scattering and SCG have been observed, generated by the accumulation of nonlinearities inside the fiber.

2. Experimental Details

The schematic setup of an ANDi-YDFL with ring configuration is shown in Fig. 1. The gain fiber was a 30 cm long Yb^{3+}-doped fiber (YDF) with a core diameter of 5 μm, and the numerical aperture of 0.2, with absorption coefficient at 976 nm of 1200 dB/m. A 976 nm laser diode (LD), used as a pump source, was coupled to the laser cavity by a wavelength-division multiplexer (WDM). The mode-locking mechanism based on the NPR technique combined two polarization controllers (PCs), and one polarization dependent isolator (PDI) inside the laser cavity. The PCs (F-POL-IL, Newport Inc.), comprising a fiber squeezer, applied simple squeeze-and-turn operations to generate a linear birefringence in the optical fiber, and induce different polarization states of the pulsed light inside the cavity by a variation of pressure. The PDI played both the role of a linear polarizer and isolator to ensure the unidirectional propagation of laser light inside the cavity. An 80/20 fiber coupler was used as an output coupler (CP), for which 20% of the laser energy was outputted. In order to prevent the feedback of pulsed light into the oscillator, an isolator was connected outside the cavity of the YDFL. Furthermore, we adopted a 95/5 coupler as a beam splitter after the isolator, in which

5% of the output light was measured by an optical spectrum analyzer (OSA, Ando AQ-6315E) and oscilloscope (Wave Surfer 62 Xs, bandwidth 650 MHz, LeCroy Inc.) to monitor the laser dynamics, and the other 95% of the output light was recorded by the detector and shown in a power meter (Newport 1918-C).

The schematic setup of the YDFA is also shown on the right hand side of Fig. 1. The employed gain fiber was a 20 m single-mode YD-GZS fiber, which was manufactured using modified chemical vapor deposition (MCVD) in conjunction with a solution doping (SD) technique, in order to achieve uniform doping of other elements, such as 20 wt% GeO_2, 1.5 wt% ZrO_2 and 0.4 wt% Yb_2O_3 [18]. The core diameter and the corresponding mode-filled diameter of the fiber were 3.25 μm and 3.75 μm, respectively [19]. The YD-GZS has high doping concentration of GeO_2 in the fiber core, third order nonlinearities including both Kerr and Raman effects for the Yb-doped germane-zirconia fiber would be greatly enhanced [20]. The incorporation of ZrO_2 can also further increase of the nonlinear optical property of silica glass based optical fibers [21], [22]–[25]. Accordingly, the YD-GZS fiber is a superior gain medium of the amplifier for the broad spectrum generation based on the cascaded Raman scattering proposed in this work in comparing to the general Yb^{3+}-doped silica fibers. The generated QML pulses from the YDFL were launched into the YDFA, and the output power and corresponding spectrum of the amplified pulse were measured by the power meter and OSA, respectively.

In comparing to the traditional soliton produced in anomalous dispersion cavity [3], the bandpass filter (BF) is a critical device for preserving the soliton inside the cavity for a PML-YDFL in ANDi cavity. However, various experimental results have demonstrated that PML pulses in ANDi cavity based on NPR mechanism can be produced without BF [5] because of the invisible filter inside laser cavity [26]. The evolution of electric field inside the PML-YDFL based on the NPR, beginning at the position *I* (P-*I*) in Fig. 1, can be represented by the Jones matrix.

$$\begin{bmatrix} E''_x(t) \\ E''_y(t) \end{bmatrix} = \begin{bmatrix} \cos\alpha_2 & 0 \\ 0 & \sin\alpha_2 \end{bmatrix} \begin{bmatrix} 1 & 0 \\ 0 & e^{-j(\Delta\varphi_L+\Delta\varphi_{NL})} \end{bmatrix} \begin{bmatrix} \cos\alpha_1 & 0 \\ 0 & \sin\alpha_1 \end{bmatrix} \begin{bmatrix} E_x(t) \\ E_y(t) \end{bmatrix} \tag{1}$$

$E_x(t)$ and $E_y(t)$ is the x- and y-component of initial *e*lectric field *E*(t) at P-*I* and $E'_x(t)$ and $E'_y(t)$ is the x- and y-component of output electric field *E''*(t) after PDL (position *II* (P-*II*)), α_1 and α_2 are the angles between *x* axis and *e*lectric field vector at the initial position and output position, relatively. Owing to the squeezing by PC and some imperfection of the SMF, the linear phase shift $\Delta\phi_L = (n_y - n_x)/\beta L$ would be produced. In addition, we need to consider the self-phase modulation (SPM) and cross phase modulation (XPM) so that the nonlinear refractive index can be expressed as:

$$n_x^{NL} = n_2\left(|E_x|^2 + \frac{2}{3}|E_y|^2\right) = n_2|E(t)|^2\left(\cos^2\alpha_1 + \frac{2}{3}\sin^2\alpha_1\right) \tag{2}$$

$$n_y^{NL} = n_2\left(|E_y|^2 + \frac{2}{3}|E_x|^2\right) = n_2|E(t)|^2\left(\sin^2\alpha_1 + \frac{2}{3}\cos^2\alpha_1\right) \tag{3}$$

Thus, the nonlinear phase shift $\Delta\phi_{NL}$ can be induced as:

$$\Delta\phi_{NL} = \left(n_y^{NL} - n_x^{NL}\right)\beta L = n_2\left(\sin^2\alpha_1 - \cos^2\alpha_1\right)|E(t)|^2\beta L/3 = -\frac{\gamma PL}{3}\cos 2\alpha_1 \tag{4}$$

Here *P* is instantaneous peak power, $\gamma(\omega_0) = n_2\,\omega_0/cA_{\text{eff}}$ is nonlinear coefficient. Based on the (1), the transmission *(T)* of the NPR can be represented by:

$$T = \frac{|E''(t)|^2}{|E(t)|^2} = \cos^2\alpha_1.\cos^2\alpha_2 + \sin^2\alpha_1.\sin^2\alpha_2 + \frac{1}{2}\sin 2\alpha_1 \sin 2\alpha_2.\cos(\Delta\phi_L + \Delta\phi_{NL}) \tag{5}$$

Here, *T* is strongly depending on $\Delta\phi_L$ and $\Delta\phi_{NL}$ and T_0 is the initial transmittance of artificial SA without incidence of the pulse ($P = 0$). Thus, an ultrafast switching can be produced after properly adjusting the PC to control α_1, α_2 and $\Delta\phi_L$ and make sure the transmittance will be increased with the intensity of input pulse.

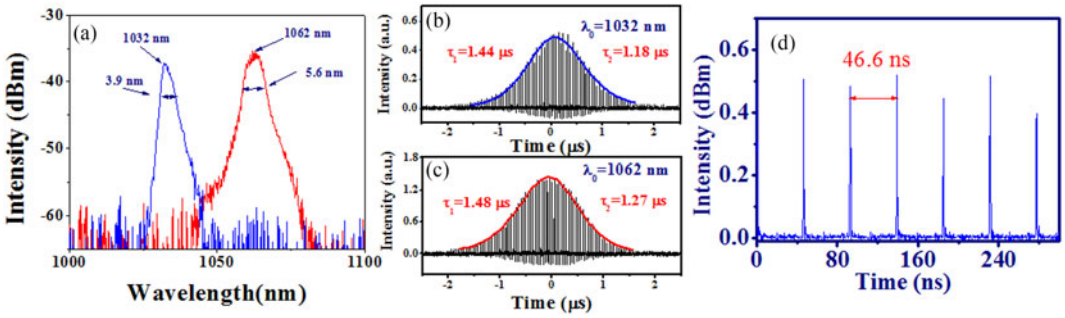

Fig. 2. (a) Optical spectra for the QML_1 (blue curve) and QML_2 (red curve) states; the corresponding time trace of single expanded Q-switched and mode-locked pulses for (b) QML_1 state (fitting curve: blue solid line) and (c) QML_2 state (fitting curve: red solid line) and (d) mode-locked pulse train inside Q-switched envelope.

In previous report, a Lyot filter [27] is adopted in PML-YDFL to control the central wavelength which based on the integration of polarization maintaining fiber (PMF) and (In-Line polarizers) (ILP). Theoretically, peak-to-peak filtering bandwidth from Lyot filter is determined by $\Delta\lambda = \lambda^2/L\,\Delta n$, where λ is center wavelength, L is the length of the PMF and $\Delta n = n_{slow} - n_{fast}$ is the birefringence. In contrast, peak wavelength of pulsed light for the PML-YDFL through the NPR can also be controlled based on invisible filter constructed by the phase shift between fast and slow axis. Here, $\Delta\phi = \Delta\phi_L + \Delta\phi_{NL} = (2\pi/\lambda).L_{eff}.\Delta n$, $L_{eff} = [1 - \exp(-\alpha L)]/\alpha$ is the effective propagation length of SMF, which L is fiber length and α is attenuation coefficient of the fiber. Owing to the tunable filter, mentioned previously, constructed by the mechanical induced birefringence change from single mode fiber [26], the central wavelength of emission light from PML fiber laser based on the NPR technique can be effectively varied.

3. Results

By proper rotation of the PCs, the YDFL could be operated in a QML state with various peak wavelengths (λ_p). Fig. 2(a) shows the optical spectra of two different states of QML pulses, where the peak wavelengths are located at 1062 nm (QML_1), and 1032 nm (QML_2), with corresponding 3-dB bandwidths ($\Delta\lambda$) of 5.6 nm and 3.9 nm, respectively. The time trace of the expanded single QML pulses for the QML_1 and QML_2 states are shown in Fig. 2(b) and (c), where the mode-locked (ML) pulses were modulated by the Q-switched envelope. In order to obtain the rising (τ_1), and falling (τ_2) times of the Q-switched envelope, we fit the curves with the formula,

$$P(t) = \frac{A}{\{\exp[1.76 \times \tau/\tau_1] + \exp[-1.76 \times \tau/\tau_2]\}^2} \tag{6}$$

where A is a scaling factor, and the temporal width and symmetric parameters of the QML envelope are defined as $\tau = (\tau_1 + \tau_2)/2$, and τ_1/τ_2, respectively [6], [7]. The determined values from a fit with (3) (red and blue solid curves) of the rising time τ_1, and falling time τ_2, of the Q-switched envelopes in Fig. 2(b) and (c), as well as the estimated temporal width, τ, and the symmetric parameters, τ_1/τ_2, are all listed in Table 1. The values indicate that the widths of the Q-switched envelopes for the QML_1 and QML_2 states are 1.31 μs, and 1.38 μs, with symmetric parameters 0.82 and 0.86, respectively. Since the estimated values of τ_1/τ_2 approach the value one, it shows that the Q-switched envelopes of the YDFL are relatively symmetric. The expansion of QML pulses in the center of the Q-switched envelope is shown Fig. 2(d). It clearly indicates that the time interval between ML pulses is around 46.6 ns, corresponded to the pulse repetition rate of 21.4 MHz, that matches well the cavity length 13.9 m.

Fig. 3 shows the evolution of the optical spectra and time traces of the YDFL QML_2 state as the pump power varies. The parameters for the evolution of QML1 state does not reveal in this paper,

TABLE 1
The Parameters of YDFL at Three QML States

States	λ_p (nm)	$\Delta\lambda$(nm)	$\tau_1(\mu s)$	$\tau_2(\mu s)$	τ_1/τ_2	$\tau(\mu s)$
Q1(QML_1)	1032	3.9	1.18	1.44	0.82	1.31
Q2(QML_2)	1062	5.6	1.27	1.48	0.86	1.37
Q3(QML_3)	1038	70	0.47	3.35	0.14	1.91

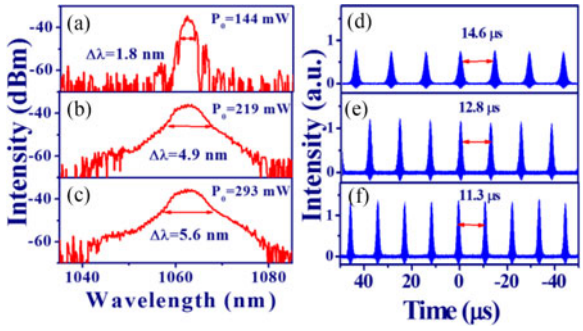

Fig. 3. The evolution of optical spectra (left hand side) (a)–(c) and the corresponded time trace of QML pulse train (right hand side) (d)–(f) of YDFL at QML_2 state as pump-power at 144 mW, 219 mW and 293 mW, respectively.

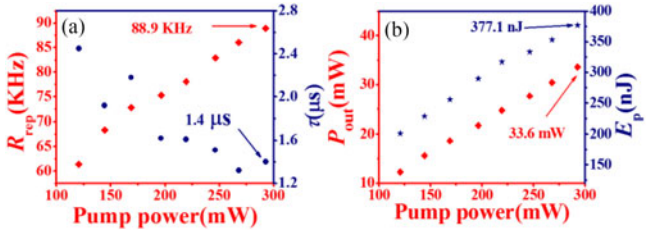

Fig. 4. The variation of (a) repetition rate (R_{rep}) and the width (τ) as well as (b) output power (P_{out}) and pulse energy (E_p) as a function of pump power for QML_2 state.

since it shows the similar characteristic with QML2 state. While the pump power increased from 144 mW to 293 mW, the 3 dB bandwidth of the optical spectrum increased from 1.8 nm to 5.6 nm, as shown in Fig. 3(a)–(c). The corresponding time traces of the Q-switched and mode-locked pulse trains, at the same pump power, are shown in Fig. 3(d)–(f). It is clear to see that the time shape of the Q-switched envelope is still relatively regular, and that the timing jitter is small for the QML_2 state. The time interval between Q-switched envelopes at a pump power of 144 mW was 14.6 μs, corresponding to a repetition rate of 68.5 kHz. As pump power was increased, the interval between Q-switched envelopes decreased (equivalently, the repetition rate increased). At a pump power of 293 mW, the interval between Q-switched envelopes was 11.3 μs, corresponding to a repetition rate of 88.5 kHz, as shown in Fig. 3(f).

The variation of the repetition rate (R_{rep}, red diamonds), and width (τ, navy points), of the Q-switched envelope as a function of pump power for the QML_2 state are shown in Fig. 4(a). The data indicates that the repetition rate and width of the Q-switched envelope increased and decreased linearly, respectively, as the pump power was increased. At the highest pump power of 292.6 mW, the repetition rate and width of envelope were 88.5 kHz, and 1.38 μs, respectively. We note that in this work, the width of the Q-switched envelope is narrower than a previously reported NPR based

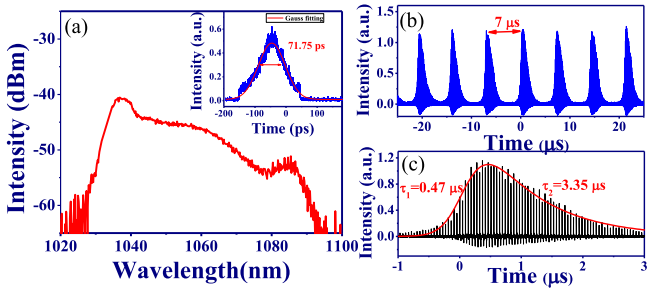

Fig. 5. (a) Optical spectrum (red solid line) as well as the inset shows the intensity autocorrelation (blue line), (b) corresponded time trace of QML pulse trains, and (c) single expanded QML pulse train at the QML_3 state.

YDFL pulse width value of 65 μs [7]. The variation in the output power, P_{out} (red diamonds), and corresponding pulse energy, E_p (blue stars), of the YDFL with increasing pump power are shown in Fig. 4(b). The highest output power and pulse energy recorded were 33.6 mW, and 377.1 nJ, respectively.

Also, a different QML state, QML_3, which was observed through adjustment of the PCs, exhibited a broad spectrum bandwidth extending from 1024 nm to 1094 nm, as shown in Fig. 5(a). The QML pulse train, shown in Fig. 5(b), indicates that the interval between Q-switched envelopes was ~7 μs, corresponding to a repetition rate of ~142.9 kHz. Through use of an autocorrelation measurement, the pulse duration of each mode-locked pulse inside the envelope was determined to be ~71.8 ps (fit with the Gaussian function). Owing to the short pulse duration of the YDFL in the QML_3 state, relatively high nonlinearity can be produced and accumulated as the ML pulsed light propagates inside the laser cavity. In addition, the period of the QML pulses in Fig. 5(b) is still observed to be relatively regular, similar to the previous states. However, the Q-switched envelope of the QML_3 state displays an asymmetric shape, and the expanded single QML pulse train is shown in Fig. 5(c). Fitting the curve with (1) reveals the rising time, τ_1, and the falling time, τ_2, of the envelope to be 0.47 μs and 3.35 μs, respectively. Furthermore, the width, τ , and the ratio, τ_1/τ_2, of the Q-switched envelope are approximately 1.91 μs and 0.14, respectively, as listed in Table 1. In comparison to the previous states, the QML_3 state exhibits a slightly broadened Q-switched envelope and a more asymmetric shape. Theoretically, the rise time τ_1 and fall time τ_2, of Q-switched envelope is related to the n_i/n_t and photon life time, respectively. Here, *n*t is threshold inversion and *n*i is initial inversion which is defined as [6]:

$$n_i = \frac{\ln(1/T_0) + \ln(1/R) + L}{\sigma l} \tag{7}$$

where T_0 is initial transmittance of SA, L is nonsaturable intracavity round-trip optical loss, σ and l are the stimulated emission cross section and the length of gain medium, R is the reflectance of laser cavity, As mentioned previously in (2) for the NPR, T_0 can be controlled by the proper controlling the polarization inside laser cavity. From (2), the initial transmittance T_0 and the loss can be controlled after proper adjusting the PC in NPR mechanism. Thus, the asymmetry shape of Q-switched envelope for the QML_3, smaller value of τ_1 and larger value of τ_2, in comparison to the previous two states can be attributed to the lower T_0 and longer photon light lifetime through artificial SA.

In comparison to the CW mode-locked pulses, the QML pulses can be used to induce nonlinearity in optical fiber due to its narrower pulse duration and lower repetition rate. Thus, we used the QML pulses (QML3) from the YDFL as a seed source, and injected it through the YDFA, using a YD-GZS fiber as the active medium, as in Fig. 1. Owing to the output power of the YDFL around 32.6 mW, the estimated intensity of each ML pulse at the QML_3 state inside the fiber is ~0.7 GW/cm^2 and the nonlinear coefficient γ of YD-GZS can be estimated to be ~19 W^{-1}Km^{-1} [19]. Here, n_2 is nonlinear refractive index 2.6 $\times$ 10^{-20} m^2/W in silica fiber and ω_0 is the center frequency of the fiber

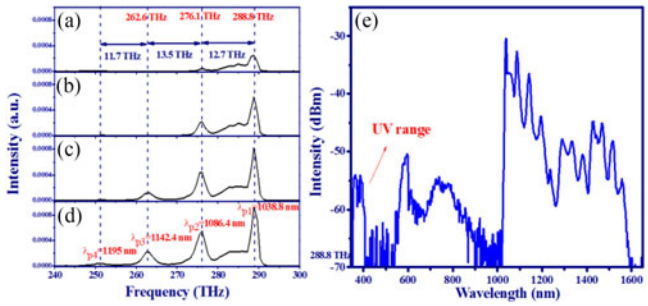

Fig. 6. Evolution of optical spectra in linear scale as the measured output power of YDFA at (a) 43.5 mW, (b) 82.5 mW, (c) 99.7 mW, and (d) 106.8 mW. (e) The generated spectrum as pump power of LD_2 at 293 mW.

laser, A_{eff} is an effective area of the silica fiber in considering the core diameter of 5 μm from the nonlinear fiber. Fig. 6(a)–(d) show the measured power spectra (linear scale) from the output port of the YDFA at four different transmitted pulse energies (from 86.1 nJ to 235.1 nJ). The emission peak of ~288.8 THz (corresponding to a peak wavelength, $\lambda_{p1} = 1038$ nm), can be observed for an LD_2 pump power of 43.5 mW. As output power increased to 82.5 mW, another emission peak at 276.1 THz (with peak wavelength $\lambda_{p2} = 1086$ nm) can be excited, about 12.7 THz downshifted in frequency relative to the λ_{p1}, of the first order Stokes wave. At even higher output powers ($LD_2 = 99.7$ mW, 106.8 mW), other emission peaks with peak wavelengths, $\lambda_{p3} = 1142.4$ nm, and $\lambda_{p4} = 1197$ nm, with relative downshifts in frequency of ~13.5 THz and ~11.7 THz, were observed (shown in Figs. 6(c) and (d)), which are close to the Raman scattering bandwidth of 13 THz. In addition to Raman scattering, other nonlinear effects such as self-phase modulation (SPM), cross phase modulation (XPM), and even the degenerate four wave mixing (DFWM), can be induced inside a single mode fiber [18]. Thus, the evolution of the optical spectrum may be shifted not only toward long wavelengths, but also toward the short wavelengths. The relative broad spectrum from visible to near IR as a pump power of 293 mW is shown in Fig. 6(e).

4. Conclusion

We investigated the characteristics of periodically Q-switched mode-locked pulses from an all normal dispersion Yb-doped fiber laser based on the nonlinear polarization rotation (NPR) mechanism. In considering the invisible filter inside cavity based on NPR, the mode-locked pulses can be generated with tunable emission wavelength after properly controlling the polarization inside cavity. In our first experimental scenario, the YDFL revealed two Q-switched envelopes with peak wavelengths of 1032 nm and 1062 nm, respectively. As pump power increased, the width of the Q-switched envelope increased, while the repetition rate decreased. Using a maximum pump power of 292.6 mW, a repetition rate of 88.5 kHz and pulse energy of 377.1 nJ were obtained. In addition, we have also demonstrated the generation of a QML state with an asymmetric Q-switched envelope, a broad spectrum bandwidth, and short pulse duration. The shape of Q-switched envelope, including the rising and falling time, is attributed to the initial population or initial transmittance of artificial SAs. Through the injection of this low repetition rate and high peak power QML pulse into a fiber amplifier, using YD-GZS fiber as the gain medium, cascaded Raman scattering was observed as the pump power was increased. As the highest LD pump power from the YDFA was set at 293 mW, a relatively broad spectrum was generated near the IR range, and some emission bands in the visible and UV regions were observed, due to the combination of various intrinsic nonlinearities.

Acknowledgment

P. H. Reddy would like to thank DST, India for the award of a Ph.D. DST - INSPIRE Fellowship (IF150744).

References

[1] K. H. Lin, J. H. Lin, and C. C. Chen, "Switchable mode-locking states in an all-fiber all-normal-dispersion ytterbium-doped laser," *Laser Phys.*, vol. 20, no. 11, pp. 1984–1989, Oct. 2010.

[2] X. Li *et al.*, "Nonlinear absorption of SWNT film and its effects to the operation state of pulsed fiber laser," *Opt. Exp.*, vol. 22, no. 14, pp. 17227–17235, Jul. 2014.

[3] X. Li *et al.*, "Single-wall carbon nanotubes and graphene oxide-based saturable absorbers for low phase noise mode-locked fiber lasers," *Sci. Rep.*, vol. 6, Apr. 2016, Art. no. 25266.

[4] M. E. Fermann, F. Haberl, M. Hofer, and H. Hochreiter, "Nonlinear amplifying loop mirror," *Opt. Lett.*, vol. 15, no. 13, pp. 752–754, Jul. 1990.

[5] J. H. Lin, D. Wang, and K. H. Lin, "High energy pulses generation with giant spectrum bandwidth and submegahertz repetition rate from a passively mode-locked Yb-doped fiber laser in all normal dispersion cavity," *Laser. Phy. Lett.*, vol. 8, no. 1, Jan. 2010, Art. no. 66.

[6] J. H. Lin, H. R. Chen, H. H. Hsu, M. D. Wei, K. H. Lin, and W. F. Hsieh, "Stable Q-switched mode-locked Nd3+: LuVO4 laser by Cr4+: YAG crystal," *Opt. Exp.*, vol. 16, no. 21, pp. 16538–16545, Oct. 2008.

[7] J. H. Lin, J. L. Jhu, S. S. Jyu, T. C. Lin, and Y. Lai, "Characteristics of a low repetition rate passively mode-locked Yb-doped fiber laser in an all-normal dispersion cavity," *Laser Phys.*, vol. 23, no. 2, Feb. 2013, Art. no. 025103.

[8] W. H. Reeves *et al.*, "Transformation and control of ultra-short pulses in dispersion-engineered photonic crystal fibres," *Nature*, vol. 424, no. 6948, pp. 511–515, Jul. 2003.

[9] J. H. Lin, K. H. Lin, C. C. Hsu, W. H. Yang, and W. F. Hsieh, "Supercontinuum generation in a microstructured optical fiber by picosecond self Q-switched mode-locked Nd: GdVO4 laser," *Laser. Phys. Lett.*, vol. 4, no. 6, pp. 413–417, Jun. 2007.

[10] F. Wang *et al.*, "Supercontinuum generation from 437 to 2850 nm in a tapered fluorotellurite microstructured fiber," *Laser. Phys. Lett.*, vol. 13, no. 12, Dec. 2016, Art. no. 125101.

[11] J. H. Lin, C. C. Taso, K. C. Hsu, K. H. Lin, and Y. Lai, "Ultrashort pulse compression for mode-locked Ti: Sapphire laser by using a tapered fiber and grating pair," *Jpn. J. Appl. Phys.*, vol. 49, no. 5, May 2010, Art. no. 052701.

[12] S. V. Smirnov, J. D. Ania-Castanon, T. J. Ellingham, S. M. Kobtsev, S. Kukarin, and S. K. Turitsyn, "Optical spectral broadening and supercontinuum generation in telecom applications," *Opt. Fiber Technol.*, vol. 12, no. 2, pp. 122–147, Apr. 2006.

[13] G. P. Agrawal, *Nonlinear Fiber Optics*, 5th ed. San Diego, CA, USA: Academic, 2013.

[14] A. Zaytsev, C. H. Lin, Y. J. You, C. C. Chung, C. L. Wang, and C. L. Pan, "Supercontinuum generation by noise-like pulses transmitted through normally dispersive standard single-mode fibers," *Opt. Exp.*, vol. 21, no. 13, pp. 16056–16062, Jul. 2013.

[15] X. Xiao and Y. Hua, "Supercontinuum generation based on all-normal-dispersion Yb-doped fiber laser mode-locked by nonlinear polarization rotation: Influence of seed's output port," *Opt. Commun.*, vol. 377, pp. 94–99, Oct. 2016.

[16] S. S. Lin, S. K. Hwang, and J. M. Liu, "Supercontinuum generation in highly nonlinear fibers using amplified noise-like optical pulses," *Opt. Exp.*, vol. 22, no. 4, pp. 4152–4160, Feb. 2014.

[17] K. H. Lin and J. H. Lin, "Amplification of supercontinuum by semiconductor and Er-doped fiber optical amplifiers," *Laser. Phys. Lett.*, vol. 5, no. 6, pp. 449–453, Jun. 2008.

[18] H. Ahmad, K. Thambiratnam, M. C. Paul, A. Z. Zulkifli, Z. A. Ghani, and S. W. Harun, "Fabrication and application of zirconia-erbium doped fibers," *Opt. Mater. Exp.*, vol. 2, no. 12, pp. 1690–1701, Dec. 2012.

[19] J. H. Lin *et al.*, "Near-infrared supercontinnum generation in single-mode nonlinear Yb3+-doped fiber amplifier," *Opt. Exp.*, vol. 22, no. 13, pp. 16130–16138, Jun. 2014.

[20] M. J. Li, S. Li, and D. A. Nolan, "Silica glass based nonlinear optical fibers," in *Proc. SPIE*, 2006, vol. 6025, Art. no. 602503.

[21] H. Ahmad, K. Thambiratnam, M. C. Paul, A. Z. Zulkifli, Z. A. Ghani, and S. W. Harun, "Fabrication and application of zirconia-erbium doped fibers," *Opt. Mater. Exp.*, vol. 2, no. 12, pp. 1690–1701, Dec. 2012.

[22] N. A. Awang *et al.*, "Supercontinuum of Zr-EDF by using Zr-EDF mode locked fiber laser," *Laser Phys. Lett.*, vol. 9, no. 1, pp. 44–49, Jan. 2012.

[23] H. Ahmad, N. A. Awang, M. C. Paul, M. Pal, A. A. Latif, and S. W. Harun, "All fiber passively mode locked Zirconium-based Erbium-doped fiber laser," *Opt. Laser Technol.*, vol. 44, no. 3, pp. 534–537, Apr. 2012.

[24] A. Hamzah *et al.*, "Passively mode-locked Erbium doped Zirconia fiber laser using a nonlinear polarisation rotation technique," *Opt. Laser Technol.*, vol. 47, pp. 22–25, Apr. 2013.

[25] H. Ahmad, M. C. Paul, N. A. Awang, S. W. Harun, M. Pal, and K. Thambiratnam, "Four-wave-mixing in Zirconia-ttria-Aluminum Erbium codoped silica fiber," *J. Eur. Opt. Soc. Rapid Public*, vol. 7, 2012, Art. no. 12011.

[26] L. Zhao, D. Tang, X. Wu, and H. Zhang, "Dissipative soliton generation in Yb-fiber laser with an invisible intracavity bandpass filter," *Opt. Lett.*, vol. 35, no. 16, pp. 2756–2758, Aug. 2010.

[27] K. Özgören and F. Ö. Ilday, "All-fiber all-normal dispersion laser with a fiber-based Lyot filter," *Opt lett.*, vol. 35, no. 8, pp. 1296–1298, Apr. 2010.